Journal of Materials Chemistry A

Nanofluidic energy conversion and molecule separation through highly stable clay-based membranes

Journal:	*Journal of Materials Chemistry A*
Manuscript ID	TA-ART-01-2019-000801.R2
Article Type:	Paper
Date Submitted by the Author:	28-Apr-2019

Complete List of Authors:	Zhou, Yi; China University of Mining and Technology - Beijing Campus, Ding, Hao; University of Connecticut, Department of Chemical & Biomolecular Engineering Smith, Andrew; University of Connecticut Jia, Xiaohui; China University of Mining and Technology - Beijing Campus Chen, Song; South China University of Technology Liu, Lan; South China University of Technology, College of Material Science and Engineering Liu, Jingjing; University of Connecticut Chavez, Sonia; University of Connecticut Hou, Zaili; University of Connecticut Cheng, Hongfei; China University of Mining and Technology - Beijing Campus, ; Chang'an University, Liu, Qinfu; China University of Mining and Technology, School of Geoscience and Surveying Engineering Sun, Luyi; University of Connecticut, Department of Chemical & Biomolecular Engineering

Nanofluidic energy conversion and molecule separation through highly stable clay-based membranes

Yi Zhou,[a,b] Hao Ding,[b] Andrew T. Smith,[b] Xiaohui Jia,[a] Song Chen,[b,c] Lan Liu,[b,c] Sonia E. Chavez,[b] Zaili Hou,[b] Jingjing Liu,[b] Hongfei Cheng,[a,d,e,*] Qinfu Liu,[a] Luyi Sun[b,*]

[a]*School of Geoscience and Surveying Engineering, China University of Mining and Technology, Beijing 100083, China.*
E-mail: h.cheng@cumtb.edu.cn
[b]*Polymer Program, Institute of Materials Science and Department of Chemical and Biomolecular Engineering, University of Connecticut, Storrs, CT 06269, USA*
Email: luyi.sun@uconn.edu
[c]*College of Materials Science and Engineering, Key Lab of Guangdong Province for High Property and Functional Macromolecular Materials, South China University of Technology, Guangzhou, 510640, China*
[d]*School of Environmental Science and Engineering, Chang'an University, Xi'an, 710054, China*
[e]*Key Laboratory of Subsurface Hydrology and Ecological Effects in Arid Region of the Ministry of Education, Chang'an University, Xi'an, 710054, China*

Abstract

Energy collection and molecule separation are two emerging applications based on membrane technologies. It remains a challenge to improve the separation performance of molecular channels. Meanwhile, the applications of membranes are typically impeded by their poor stability under practical hydrous conditions. Herein, we present the fabrication of a uniformly lamellar membrane using montmorillonite nanosheets as building blocks. We managed to achieve nanofluidic ion transport and molecule separation simultaneously. The membrane nanochannels possess nanofluidic ion transport properties with an output power density up to 0.18 W m^{-1} at a membrane thickness of 11.2 μm under a 1000-fold transmembrane concentration difference. The membrane also shows water permeance of 429 L m^{-2} h^{-1} atm^{-1} at a thickness of 2.5 μm and high separation efficiency for both cationic and anionic dyes. Moreover, the montmorillonite-based membranes can maintain a high stability in aqueous conditions under soaking, shaking, and even ultrasonication.

Keywords: Nanochannels, energy conversion, molecule separation, water-stability, clay mineral

Introduction

Energy utilization and technological developments have been the foundation for human progress throughout human history.[1] Traditional non-renewable energy reserves are declining, and the continued reliance on fossil fuels have led to widespread environmental issues.[2] Therefore, the transformation and utilization of new energy sources is extremely urgent. In addition to solar,[3] thermal,[4] and hydrogen energy[5] that have been extensively studied, renewable energies contained in water system are also of great interest, including mechanical energy of flowing water[6] and potential chemical energy of water salinity.[7] In energy conversion of salinity gradients, the traditional method is to mix seawater and river water through an ion exchange membrane with selective permeability, during which the salinity gradient energy is obtained by reverse electroosmosis technology.[8] But it suffers a low power density and a high power generation cost, limiting its widespread adoption.[7] With the development of artificial energy conversion devices, the use of solid nanopores with regular geometry and charge selectivity instead of conventional ion exchange membranes to collect salinity gradient energy has gained high attention.[9-12] Two-dimensional (2D) lamellar membranes with millions of confined nanochannels show great potential in energy conversion and power generation.[13-16] The confined space in the nanochannels with a typical size on the order of 1-100 nm, which is comparable to the Debye length,[17] can drastically change the behavior of the nanofluid in fully wetted 2D membrane materials.[18-20]

Membrane-based technologies not only have great potential in harvesting green

energy, but also play an important role in water purification because of their water transport properties and molecular sieving capabilities.[21-23] Molecular rejection for nanochannels of the membranes involves both charge-specific separation and physical size cut-off.[24] Nanoscale wrinkles, exposed functional groups inside the channel, and molecules externally introduced into the channels are regularly considered as the support pillars to construct nanochannels, but are also seen as a barrier to permeation.[25] Many 2D nanoplatelets have been chosen to prepare lamellar membranes for harvesting energy and purifying water, including graphene, MoS_2, and MXenes.[23, 26-28] However, it is highly desirable to explore more environmentally-friendly and cost-effective alternatives, which possess a monolayer structure, high mechanical strength, and robust chemical stability without sacrificing high efficiency, for various applications.

Clays are the most abundant naturally occurring phyllosilicate minerals in the earth's crust.[29] To some extent, unlike other minerals, clays are sustainable because weathering and hydrothermal alteration constantly generate clays at a rate much faster than the formation of other minerals.[30] Clays have already shown significant potential as nanosheet building blocks for the reconstruction of lamellar membranes because of their ease of exfoliation, high chemical and thermal stability, and structural diversity.[31-37] In general, the thickness of most individual single-layer clay nanosheets (in ~1-12 nm range[14, 33, 38]) is larger than that of GO sheets while their lateral dimensions (in ~300-1000 nm range[14, 39-42]) is smaller. Fast transport of molecules depends on regular and straight nanochannels, which allows for continuous and steady molecular-flow.[43]

Meanwhile, small width distribution of the nanochannels is the key to high membrane rejection.[44]

In this work, we choose montmorillonite (MMT) as the model building blocks to assemble 2D nanofluidic channels with decent energy conversion and molecule separation. Compared with other clays, MMT is much easier to be exfoliated into individual nanosheets, be modified to obtain desired surface properties, and be assembled into functional membranes.[45-48]

Experimental

Reconstruction of MMT nanosheets

MMT is a hydrated sodium calcium aluminum magnesium silicate hydroxide, (Na, $Ca)_{0.33}(Al\ Mg)_2(Si_4O_{10})(OH)_2 \cdot nH_2O$. Na^+ MMT is produced by the cation exchange of Ca^{2+} by Na^+. In addition, the Al and Si in the structure are often substituted by Fe/Mg and Al, respectively.[49] A sample of 400 mg of Na^+ MMT powders (from Minerals Technologies Inc.) was dispersed in 100 mL deionized (DI) water and then ultrasonicated for 2 h to obtain a uniform MMT dispersion. A sample of 200 mg of cetyltrimethylammonium bromide (CTAB, from Sigma-Aldrich) was dissolved in 40 mL DI water with the assistance of ultrasonication. Then the MMT dispersion and CTAB solutions were mixed with 100 mL ethanol under stirring for 2 h at 70 ℃ in a water bath, during which the exfoliated MMT nanosheets were readily modified by CTAB. A precipitate formed after alternatively washing with DI water and ethanol. Eventually, the

precipitate was dispersed in 100 mL of ethanol with the assistance of stirring for 24 h to obtain the CTAB modified MMT dispersion.

The dispersion of the CTAB modified MMT (ca. 2.0 mg/mL) was filtrated through a nylon filter (47 mm in diameter, 0.2 μm in pore size, from Whatman) to form a reconstructed MMT membrane (RMM). The RMM was subsequently dried in air at room temperature to remove residual water. The flexible thin film can be readily removed from the nylon substrate. The thickness of the RMM can be easily controlled by varying the volume of the dispersion. Control MMT membranes were also fabricated via the same approach using non-modified MMT nanosheets.

Characterization

The microstructure of the RMMs was characterized by a field emission scanning electron microscope (FE-SEM, FEI NOVA NanoSEM 450). X-ray diffraction patterns were recorded on an X-ray diffractometer (Bruker D5005) with Cu Kα radiation (λ=0.154 nm) operating at 40 kV and 40 mA. Transmission electron microscopy (TEM) imaging was performed on a JEOL 2010 TEM (Tokyo, Japan) with an accelerating voltage of 200 kV. Atomic force microscopy imaging was performed on Asylum Research AFM (MFP-3D). The hydrophilicity of the membrane surface was tested by a contact angle goniometer (ramé-hart Model 100). UV-Vis spectra of the dyes were acquired on a UV-Vis spectrophotometer (Lambda 900, PerkinElmer) from 400 to 800 nm. Zeta potential measurements were performed on a Malvern Zetasizer (NanoZS90) using a dispersion of 0.10 mg/mL. FTIR characterization was conducted on a PerkinElmer Spectrum 100

spectrophotometer to identify the existence of CTAB in the RMMs.

Electrical

A piece of RMM was clamped in between a custom-built two-compartment electrochemical cell (Figure 4a inset and 4c inset). The electrolyte reservoirs are large enough that a significant membrane potential is not built up to oppose the cationic flow during the electrochemical measurement. The resulting ionic current was recorded with a source meter (Keithley 2400) through a pair of Ag/AgCl electrodes. The test area is 0.2 mm^2 for ion transport and salinity gradient energy conversion.

Water permeability and dye rejection of the RMMs

UV-visible spectra were used to evaluate the rejection performance of the RMMs for various dyes. Methylene blue (MB), methyl orange (MO), and rhodamine B (RB) were chosen to permeate the RMMs on a home-made dead-end vacuum filtration device with an effective area of 4.0 cm^2 under a pressure difference of 1.0 atm at room temperature. The volume of feed solution (5.0 μM) was 10.0 mL.

The permeance J (L m^{-2} h^{-1} atm^{-1}) and rejection R (%) were calculated by using Equations (a) and (b), respectively:

$$J = \frac{V}{A\Delta tP} \qquad \text{(a)}$$

$$R = 1 - \frac{C_p}{C_f} \times 100\% \qquad \text{(b)}$$

where V (L) is the volume of permeated water, A (m^2) is the effective membrane area, Δt (h) is the permeation time, P (1.0 atm) is the pressure difference, and C_p and C_f are the concentrations of penetrate and feed solution, respectively.

Results and discussion

Herein, we report the design and fabrication of a 2D highly stable clay-based membrane that can be used for both salinity gradient energy conversion and organic dyes/water separation. The reconstruction process is illustrated in **Figure 1a** and Figure S1. Montmorillonite (MMT) is a typical 2:1 layered silicate clay mineral. The unit cell is composed of an alumina octahedral sheet sandwiched by two silica tetrahedral sheets. In our work, first, Na^+ MMT was dispersed in DI water with the assistance of stirring, followed by 30 min of ultrasonication, to obtain exfoliated MMT nanosheets. The exfoliation of Na^+ MMT can be readily achieved by ultrasonication because of the weak interlayer interaction, negative net layer charge, and the existence of exchangeable Na^+ ions between the layers.[38, 40, 50] Afterward, the MMT nanosheets were modified by mixing with a cationic surfactant, cetyltrimethylammonium bromide (CTAB), in water at 65 °C for 2 h. Finally, a reconstructed MMT membrane (RMM) was formed after vacuum filtration of the modified MMT dispersion by using a nylon filter. Figure 1b schematically illustrates the structure of the RMM. As an ionic compound, CTAB completely ionizes in water.[51] The resulting CTA^+ cation is a positively charged tetrahedron with a long hydrophobic tail, attached on both sides of the negatively charged

MMT nanosheets, forming a pillar-like structure in between 2D nanochannels. [52, 53]

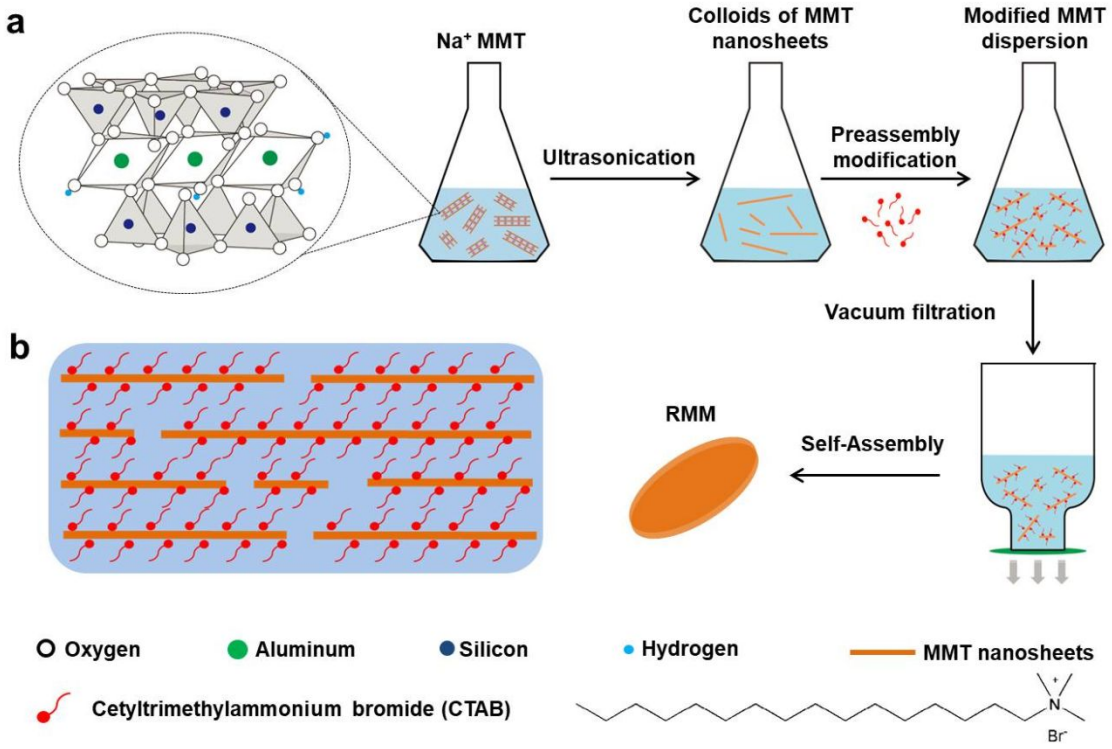

Figure 1. Fabrication of RMM. (a) Structure of MMT and fabrication processes from MMT to RMM, including exfoliation, modification, vacuum filtration, and self-assembly. (b) Schematic of the formed RMM.

The lateral dimensions of the exfoliated MMT nanosheets are from dozens of microns to hundreds of microns based on TEM characterization (**Figure 2a**). The AFM characterization revealed the morphology of a representative CTAB modified MMT nanosheet (Figure 2b) with a thickness of ca. 2.2 nm (Figure 2c). Since the thickness of a single-layer MMT nanosheet is ca. 1.0 nm[54] and the thickness of an individual CTAB layer is ca. 0.4 nm (Figure S2), considering the electrostatic interactions between MMT

and CTAB, it is expected that one or more layers of CTAB molecules are adsorbed on both sides of MMT nanosheets. The AFM image (Figure S3a) and the height profiles (Figure S3b) of the RMM show the morphology of a typical membrane surface. Pristine MMT nanosheets were negatively charged with a zeta potential of -33.1 mV at pH 7. Upon modification with CTAB, a positive shift to -27.3 mV in zeta potential was observed (Figure 2d), because partial negative charges of MMT nanosheets were balanced by the positive charges of quaternary ammonium ions. The result suggests that most negative charges still retained. Moreover, the hydroxyl groups on the edge of MMT nanosheets are hydrophilic,[55, 56] namely, water is encouraged to enter the nanochannels through the entrance.[57]

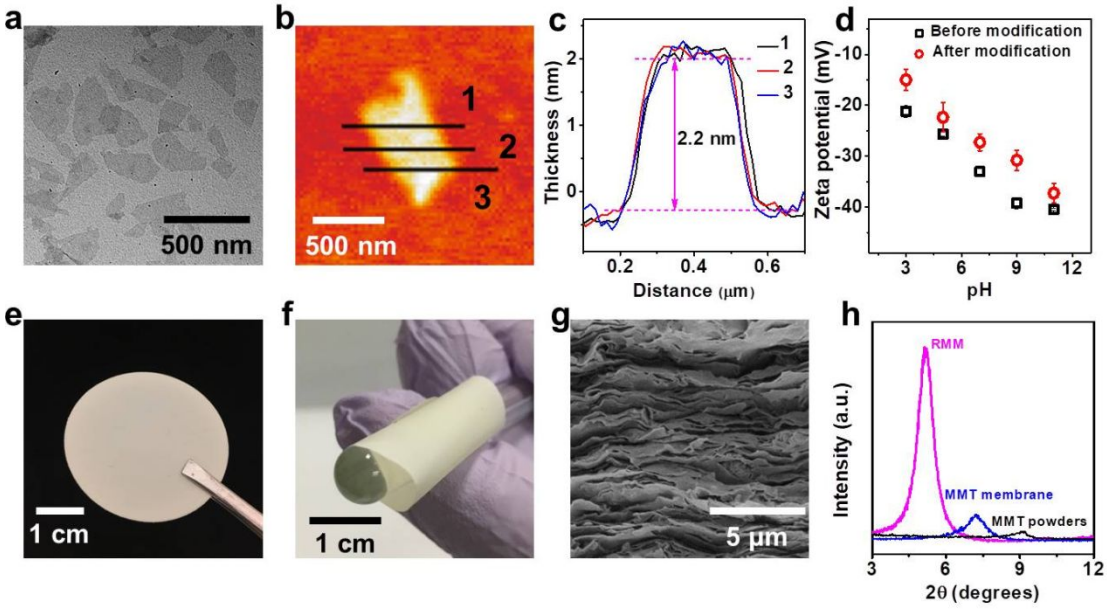

Figure 2. Characterizations of RMM. (a) TEM image of the exfoliated MMT. (b) AFM image and (c) height profile of a representative CTAB modified MMT nanosheet. (d) Zeta potential of the MMT dispersion before and after CTAB modification. (e) Digital picture of an RMM, a free-standing macroscopic membrane. (f) Digital picture of a scrolled RMM. (g) SEM image of the cross-section of an RMM showing a lamellar structure. (h) XRD patterns of MMT powders, an MMT membrane, and an RMM.

The exfoliated 2D MMT nanosheets can be restacked into a membrane through a facile vacuum filtration process. The paper-like, free-standing RMM (Figure 2e) can be readily removed from the nylon support. The free-standing RMM also possesses a high flexibility; it remains intact when rolled on a glass rod with a diameter of 35 mm (Figure 2f). Tensile tests were performed on both the RMMs and neat MMT membranes (Figure S4). Compared with the neat MMT membranes, it is clear that the chemical modification can enhance the mechanical properties of RMMs, because the electrostatic adsorption between MMT nanosheets and CTAB, and the degree of entanglement between carbon chains are positively correlated with the content of CTAB.[14, 58] The RMM exhibits a well-ordered lamellar structure according to the SEM characterization (Figure 2g). The chemical composition of MMT can be confirmed by the energy dispersive X-ray spectroscopy mapping on the cross section of an RMM (Figure S5). The results show that the content of oxygen is the highest, and the content of silicon is roughly twice of that of aluminum, which is consistent with the ratio of the two elements in the MMT crystal structure. We then used XRD to characterize the layered structure of the pristine MMT powders, MMT membrane, and RMM (Figure 2h). The pristine MMT powders show a diffraction peak at 9.1°, corresponding to an interlayer distance of 0.97 nm, attributed to the original bulk stacking and the trapped water molecules between the stacked MMT nanosheets.[40, 59] The restacked MMT membrane shows a peak at 7.3°, corresponding to an interlayer spacing of 1.22 nm, which suggests that the nanochannels are fully

hydrated. After modification with CTAB, the RMM shows a strong diffraction peak at 5.2°, corresponding to an interlayer distance of 1.71 nm. The larger interlayer distance implies that CTAB molecules were successfully embedded between the reconstructed MMT neighboring nanosheets as spacers. By comparing the FTIR spectra of the MMT and RMM, shown in Figure S6, two new vibration bands at 2926 and 2847 cm^{-1} were observed, which can be assigned to the symmetric and asymmetric stretching vibrations of $-(CH_2)_n-$, further supporting the presence of CTAB in the membrane structure.

The RMMs show an extraordinary stability in water. Before modification with CTAB, the MMT membrane was hydrophilic with a surface contact angle of 66.5° (Figure S7a), consistent with the hydrophilic nature of bulk MMT. The MMT membranes are very difficult to remove from the nylon support. When the membranes with the nylon substrate were soaked in water, they were easily swollen and then disintegrated in water quickly with a slight shake, which is expected (Figure 3a and b). After 30 s of ultrasonication, the restacked MMT membranes were well dispersed in water, only the nylon support remained (Figure 3c). But after modification with CTAB, the RMMs turned to be hydrophobic with a surface contact angle of 105.1° because of the exposed hexadecyl chains of CTAB on the surface (Figure S7b). In contrast, when the RMMs were soaked in water, they stayed intact for more than 6 months (Figure 3d, g, and j). More surprisingly, no visible damage or delamination was observed when the RMMs were shaken in water for more than 24 h (Figure 3e, h, and k), and only negligible damage was observed after ultrasonication for more than 5 min (Figure 3f and i). The

RMMs were eventually damaged after 10 min of ultrasonication. We also recorded XRD patterns of the RMM before and after hydration (Figure S8). The hydration only led to a very marginal increase in interlayer distance, showing a highly stable microstructure. The RMMs can also maintain their original structure in strong acidic and basic solutions for months (Figure S9). High stability in various solvents is essential for many liquid-phase applications of the RMMs.

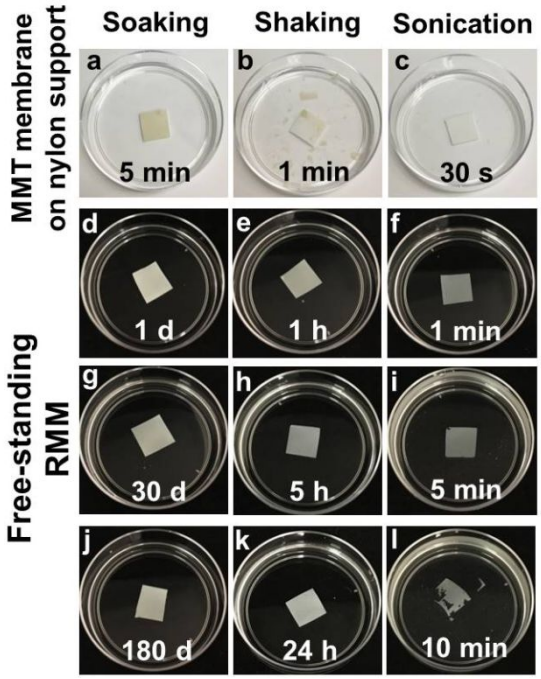

Figure 3. High stability of the RMMs in water. (a-c) Stability of an MMT membrane on a nylon support under soaking, shaking, and ultrasonication for 5 min, 1 min, and 30 s, respectively. (d), (g), and (j) Stability of a free-standing RMM under soaking for 1, 30, and 180 d, respectively. (e), (h), and (k) Stability of a free-standing RMM under shaking for 1, 5, and 24 h, respectively. (f), (i), and (l) Stability of a free-standing RMM under ultrasonication for 1, 5, and 10 min, respectively.

The RMMs with a thickness of 11.2 μm were used to investigate the ion transport properties by using Ag/AgCl electrodes to measure the current-voltage (*I*-*V*) responses

across the membrane in potassium chloride (KCl) electrolyte (Figure 4a inset). Representative *I-V* characteristics through the RMMs are linear in KCl solutions of various concentrations (Figure 4a). Generally, the conductance is proportional to the concentration of bulk solution.[18] When a solid surface is exposed to a fluid, the counter ion is attracted due to the presence of solid surface charge, resulting in a greater counter ion concentration near the solid surface than that of the bulk solution. At the same time, a counter ion concentration gradient is generated, which diffuses from the solid surface to the bulk solution. This structure is called an electrical double layer (EDL). For the RMM transmembrane system, at high salt concentrations, because of the very thin EDL in the nanochannels, the ionic conductance is determined by the concentration of the bulk electrolyte solution. While at lower concentrations of below 10^{-1} M (Figure 4b), due to the overlap of EDL, this ionic conductance begins to deviate from bulk behavior and then converges to a saturated value, showing strong surface charge controlled ion transport properties.[14, 19, 20] Estimated based on the Debye-Hückel approximation, the height of the 2D nanochannels should be greater than 1 nm and less than 3 nm,[14, 17] which is consistent with XRD results shown in Figure 2h.

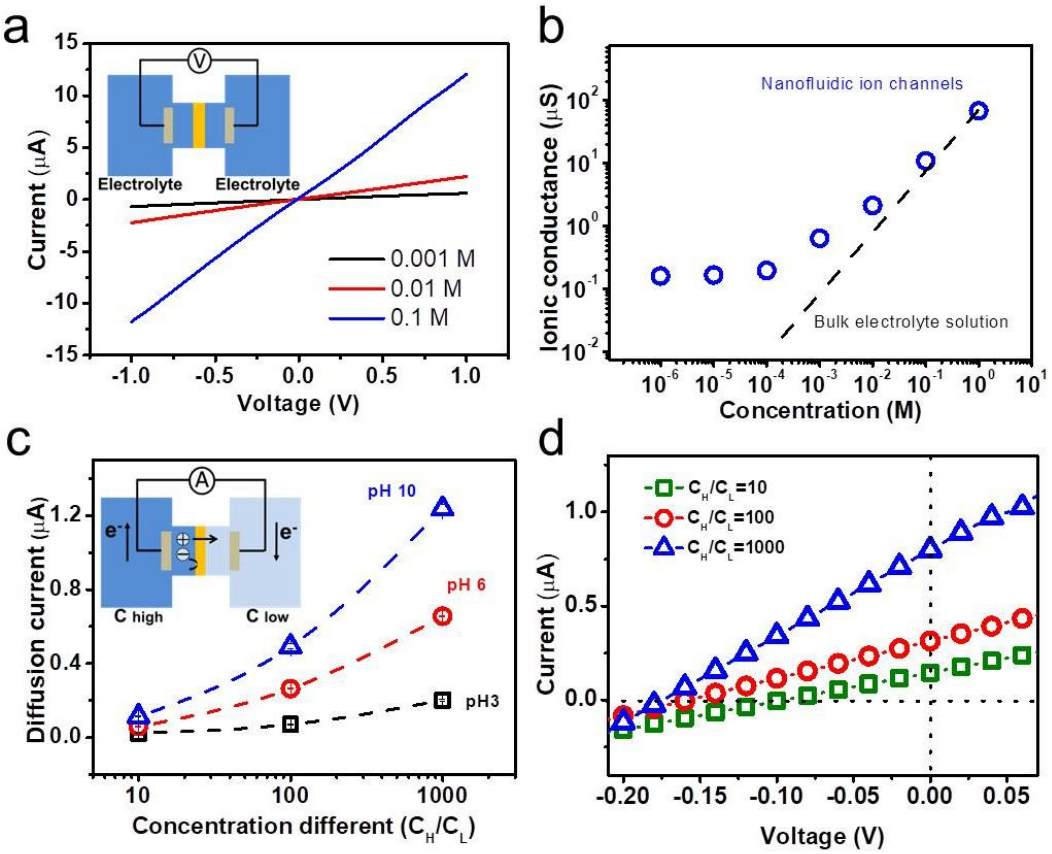

Figure 4. Ionic transport properties of the RMM. (a) Representative I-V curves through the nanochannels at different KCl concentrations. Inset: scheme of the experimental setup. (b) Transmembrane ionic conductance as a function of electrolyte concentration. (c) Measured diffusion current at pH values of 3.0, 6.0, and 10.0 under salt concentration gradient. Inset: scheme of the experimental setup. (d) Power generation for the RMM with salt concentration gradients of 10, 100, and 1000.

To further confirm the ion selectivity of the negatively charged RMM, net diffusive ionic current was recorded without externally applied voltage (Figure 4c inset). Three salts concentration gradients (C_{high}/C_{low} = 10, 100, and 1000, C_{low} = 1.0 mM) across the RMM at pH 3, 6, and 10 were investigated. As shown in Figure 4c, the magnitude of the diffusion current increased as the applied concentration gradient was changed from 10- to 1000-fold. The increase in pH led to a stronger surface charge which promoted the

generation of diffusion current as well (Figure 2d).[14]

The osmotic power generation was tested by measuring the electroosmotic potentials and currents with various KCl concentration gradients across the RMMs. As shown in Figure 4d, both the open-circuit voltage (U_{OC}: intercepts on the Voltage axis) and short-circuit current (I_{SC}: intercepts on the Current axis) increase along with a rise of salt concentration gradient from 10- to 1000-fold. We also observed that the direction of the measured diffusion current was consistent with the net flow of the positive charges from high- to low- concentration reservoirs, which also suggests that the nanochannels are cation-selective.[60] The maximum output electric power (P_{max}) can be directly calculated using the equation $P_{max} = U_{OC} \times I_{SC}/4$. Under very weak acidic conditions (pH ≈ 6), the output power density of the energy harvesting system was estimated to be 0.18 W m^{-2} under 1000-fold salt concentration gradient (Figure S10). Moreover, the cation transference number (t_+) of the RMM approaches 0.93 under 10-fold salt concentration difference, corresponding to an electrochemical energy conversion efficiency of ca. 35.3% (Supporting Information), which is comparable with other 2D material systems in salinity energy conversion.[13, 14, 20, 61]

To further confirm the selective behavior for small organic molecules through the nanofluidic channels of the RMMs, we also tested the permeability and separation performance through pressure-driven filtration. The permeability of the RMMs with a thickness from 2.5 to 8.7 μm was investigated (Figure S11). The water permeance decreased (from 750 to 33 L m^{-2} h^{-1} atm^{-1}) exponentially with an increase of the RMM

thickness, which is consistent with other separation membranes due to the increase of mass transfer resistance.[22] Figure 5 summarizes the separation performance of the RMMs for various dyes. It can be found that the permeance of MB (1.6×0.8 nm in dimensions[62]) and MO (1.6×1.0 nm in dimensions[63]) solution shows a similar value, which is much higher than that of RB (1.8×1.4 nm in dimensions[44]) solution (Figure 5a). For the rejection in Figure 5b, although water permeance decreased, the dye rejection increased with an increase in membrane thickness. The rejections for RB reached 94%, 96%, and 99% with a thickness of 2.5, 3.6, and 6.4 μm, respectively, which is much higher than that for MB and MO. This is mainly because RB molecules have a comparable size with the nanochannels in RMMs (and much larger than MB and MO), and thus they are more likely to block the nanochannels, leading to low permeance and high rejection.[44, 62]

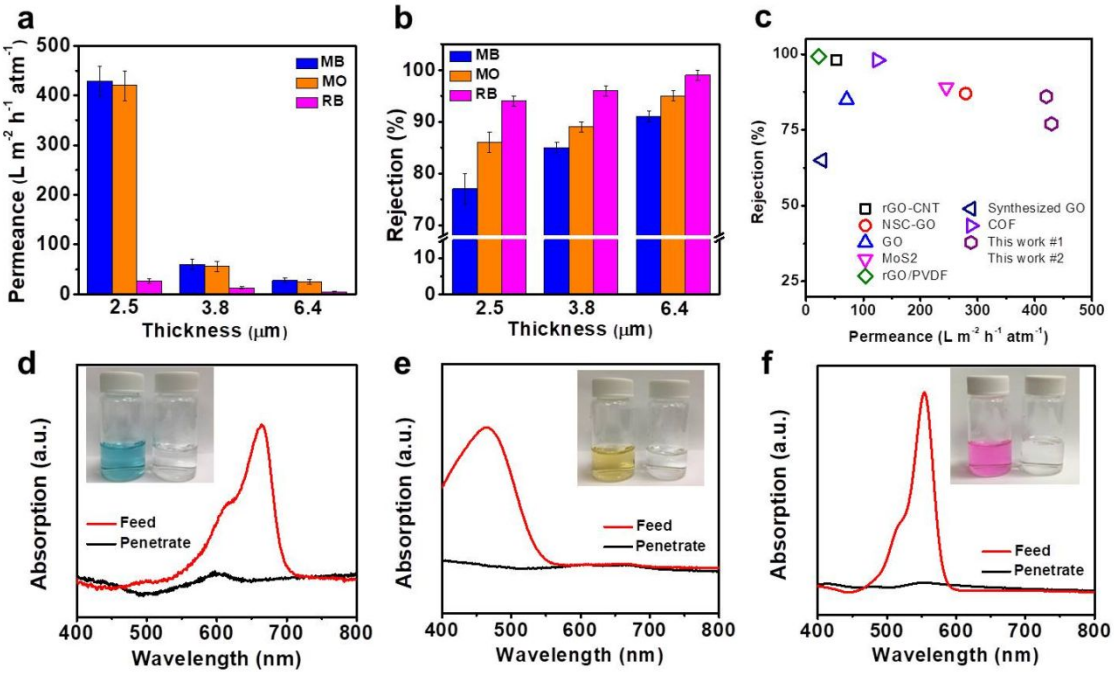

Figure 5. Separation performance of the RMMs. (a) Permeance of MB, MO, and RB (organic dyes: 5 μM) through the RMMs with a thickness of 2.5, 3.8, and 6.4 μm. (b)

Rejection of MB, MO, and RB of the RMMs with a thickness of 2.5, 3.8, and 6.4 μm. (c) Permeance and rejection comparison of the RMM with other separation membranes reported in the literature.[62, 64-69] UV-vis absorption spectra and photographs of the feed and the permeate of (d) MB, (e) MO, and (F) RB solution after filtration by the RMM (6.4 μm).

The rejection for positively charged MB is much lower than that for negatively charged MO. In general, the positively charged molecules are easier to be taken up by negatively charged membranes via electrostatic interactions. As a result, the nanochannels are easier to be blocked, resulting in a higher rejection for cationic dyes.[64] However, in our system, since the CTAB molecules serve as pillars in the structure of the nanochannels, when the negatively charged MO molecules pass through, the CTA^+ cations coagulation occurs due to electrostatic adsorption, leading to clog of the channels. The results indicate that electrostatic interaction in the interlayer space dominates the adsorption of the dye molecules. Note that the weak electrostatic repulsion between negatively charged dyes and RMMs could promote their rejection to some extent as well.[27] The positively charged MB molecules are adsorbed on the negatively charged MMT surface and do not block the channels, thus having a lower rejection (Figure 5b). The 2.5 μm thick RMM shows a water permeance of 429 L m^{-2} h^{-1} atm^{-1}, higher than that of some reported membranes with an even lower thickness. Meanwhile, the rejection performance also reached the average level of the separation membranes in the literature (Figure S12 and Figure 5c). In addition, most of the nanochannels in the RMM are hydrophobic due to the existence of CTA^+, which creates slip flow boundary conditions

inside the nanochannels to enhance the fluidic velocity.[70] Moreover, the hydroxyl groups on the edge of MMT nanosheets are hydrophilic, while the nanochannels are hydrophobic; the alternating hydrophobic and hydrophilic nanochannels can further promote the permeance.[71] Figure 5d-f show the typical rejection performance of 6.4 μm-thick RMMs. The UV-visible absorption spectra of the feed and penetrate solutions show significant differences before and after filtration through the RMMs. The color of the three feed solutions also changed from blue (MB), yellow (MO), and pink (RB) to colorless, showing a nearly perfect separation performance.

Conclusions

In summary, we prepared free-standing MMT-based membranes with nanofluidic energy conversion behavior and high separation efficiency by restacking modified individual MMT nanosheets. The modifier CTAB not only supports the nanochannels as pillars, but also plays a significant role in capturing dye molecules. The RMMs showed a high stability in water under soaking, shaking, and even brief ultrasonication conditions. The RMMs can be used for salinity gradient energy conversion. An output power density of 0.18 W m^{-2} was achieved under a 1000-fold salt concentration gradient at a membrane thickness of 11.2 μm. These membranes also showed water permeance of 429 L m^{-2} h^{-1} atm^{-1} at a thickness of 2.5 μm, higher than other membranes with a same thickness. They also show high separation efficiency to both positive and negative dyes. The combination of nanofluidic ionic transport and molecule separation through 2D channels presents

valuable features to create new smart multifunctional membranes that can be used for collecting energy while purifying wastewater.

Conflicts of interest

There are no conflicts to declare.

Acknowledgements

The authors acknowledge the support by the National Science Foundation (CMMI-1562907) and the Kaneka Corporation. Q.L. thanks the support by the Science and Technology Major Projects of Shanxi Province of China (Project Number: 20181101003). Y.Z. thanks the support from the China Scholarship Council (CSC).

References

1. D. Lindley, *Nature*, 2009, **458**, 138-141.
2. S. Pacala and R. Socolow, *Science*, 2004, **305**, 968-972.
3. B. Tian, X. Zheng, T. J. Kempa, Y. Fang, N. Yu, G. Yu, J. Huang and C. M. Lieber, *Nature*, 2007, **449**, 885.
4. A. J. Minnich, M. S. Dresselhaus, Z. F. Ren and G. Chen, *Energy & Environmental Science*, 2009, **2**, 466-479.
5. S. Dunn, *International Journal of Hydrogen Energy*, 2002, **27**, 235-264.
6. H. Daiguji, P. Yang, A. J. Szeri and A. Majumdar, *Nano Letters*, 2004, **4**, 2315-2321.
7. J. N. Weinstein and F. B. Leitz, *Science*, 1976, **191**, 557-559.
8. J. Veerman, M. Saakes, S. J. Metz and G. J. Harmsen, *Journal of Membrane Science*, 2009, **327**, 136-144.
9. W. Guo, L. Cao, J. Xia, F.-Q. Nie, W. Ma, J. Xue, Y. Song, D. Zhu, Y. Wang and L. Jiang, *Advanced Functional Materials*, 2010, **20**, 1339-1344.
10. W. Guo, H. Xia, F. Xia, X. Hou, L. Cao, L. Wang, J. Xue, G. Zhang, Y. Song, D.

Zhu, Y. Wang and L. Jiang, *ChemPhysChem*, 2010, **11**, 859-864.
11. D.-K. Kim, C. Duan, Y.-F. Chen and A. Majumdar, *Microfluidics and Nanofluidics*, 2010, **9**, 1215-1224.
12. F. Zhan, Z. Wang, T. Wu, Q. Dong, C. Zhao, G. Wang and J. Qiu, *Journal of Materials Chemistry A*, 2018, **6**, 4981-4987.
13. J. Ji, Q. Kang, Y. Zhou, Y. Feng, X. Chen, J. Yuan, W. Guo, Y. Wei and L. Jiang, *Advanced Functional Materials*, 2017, **27**, 1603623.
14. H. Cheng, Y. Zhou, Y. Feng, W. Geng, Q. Liu, W. Guo and L. Jiang, *Advanced Materials*, 2017, **29**, 1700177.
15. W. Guo, C. Cheng, Y. Wu, Y. Jiang, J. Gao, D. Li and L. Jiang, *Advanced Materials*, 2013, **25**, 6064-6068.
16. F. Yan, L. Yao, K. Chen, Q. Yang and B. Su, *Journal of Materials Chemistry A*, 2019, **7**, 2385-2391.
17. W. Sparreboom, A. van den Berg and J. C. T. Eijkel, *Nature Nanotechnology*, 2009, **4**, 713.
18. K. Raidongia and J. Huang, *Journal of the American Chemical Society*, 2012, **134**, 16528-16531.
19. D. Stein, M. Kruithof and C. Dekker, *Physical Review Letters*, 2004, **93**, 035901.
20. K. Xiao, P. Giusto, L. Wen, L. Jiang and M. Antonietti, *Angewandte Chemie*, 2018, **130**, 10280-10283.
21. W. J. Koros and C. Zhang, *Nature Materials*, 2017, **16**, 289.
22. K. H. Thebo, X. Qian, Q. Zhang, L. Chen, H.-M. Cheng and W. Ren, *Nature Communications*, 2018, **9**, 1486.
23. Q. Yang, Y. Su, C. Chi, C. T. Cherian, K. Huang, V. G. Kravets, F. C. Wang, J. C. Zhang, A. Pratt, A. N. Grigorenko, F. Guinea, A. K. Geim and R. R. Nair, *Nature Materials*, 2017, **16**, 1198.
24. L. Huang, J. Chen, T. Gao, M. Zhang, Y. Li, L. Dai, L. Qu and G. Shi, *Advanced Materials*, 2016, **28**, 8669-8674.
25. L. Qiu, X. Zhang, W. Yang, Y. Wang, G. P. Simon and D. Li, *Chemical Communications*, 2011, **47**, 5810-5812.
26. W. J. Koros and C. Zhang, *Nature Materials*, 2017, **16**, 289.
27. J. Wang, P. Chen, B. Shi, W. Guo, M. Jaroniec and S.-Z. Qiao, *Angewandte Chemie International Edition*, 2018, **57**, 6814-6818.
28. S. Rajesh, Y. Zhao, H. Fong and T. J. Menkhaus, *Journal of Materials Chemistry A*, 2017, **5**, 4616-4628.
29. G. Lagaly, M. Ogawa and I. Dékány, *Journal*, 2006.
30. L. Heller-Kallai, *Developments in Clay Science*, 2006, **1**, 289-308.
31. G. K. Dedzo and C. Detellier, *Advanced Functional Materials*, 2018, **28**, 1703845.
32. J. Liu and G. Zhang, *Physical Chemistry Chemical Physics*, 2014, **16**, 8178-8192.
33. J.-J. Shao, K. Raidongia, A. R. Koltonow and J. Huang, *Nature Communications*,

2015, **6**, 7602.
34. Y. Zhou, A. M. LaChance, A. T. Smith, H. Cheng, Q. Liu and L. Sun, *Advanced Functional Materials*, 2019, DOI: 10.1002/adfm.201807611.
35. Y. Xu, Y. Zhou, J. Liu and L. Sun, *Journal of Energy Chemistry*, 2017, **26**, 1026-1029.
36. S. Zhang, Q. Liu, Y. Yang, D. Wang, J. He and L. Sun, *Applied Clay Science*, 2017, **147**, 117-122.
37. S. Zeng, D. Zhang, W. Huang, Z. Wang, S. G. Freire, X. Yu, A. T. Smith, E. Y. Huang, H. Nguon and L. Sun, *Nature Communications*, 2016, **7**, 11802.
38. F. Ding, J. Liu, S. Zeng, Y. Xia, K. M. Wells, M.-P. Nieh and L. Sun, *Science Advances*, 2017, **3**, e1701212.
39. R. K. Gogoi and K. Raidongia, *Advanced Materials*, 2017, **29**, 1701164.
40. T. Xiao, Q. Liu, Q. Zhang, Z. Liu and J. Zhai, *The Journal of Physical Chemistry C*, 2017, **121**, 18954-18961.
41. J. Peng, Y. Cheng, A. P. Tomsia, L. Jiang and Q. Cheng, *ACS Applied Materials & Interfaces*, 2017, **9**, 24993-24998.
42. M.-L. Liu, M. Huang, L.-Y. Tian, L.-H. Zhao, B. Ding, D.-B. Kong, Q.-H. Yang and J.-J. Shao, *ACS Applied Materials & Interfaces*, 2018, **10**, 44915-44923.
43. J. Shen, G. Liu, K. Huang, Z. Chu, W. Jin and N. Xu, *ACS Nano*, 2016, **10**, 3398-3409.
44. H. Huang, Z. Song, N. Wei, L. Shi, Y. Mao, Y. Ying, L. Sun, Z. Xu and X. Peng, *Nature Communications*, 2013, **4**, 2979.
45. D. Zhang, B. L. Williams, E. M. Becher, S. B. Shrestha, Z. Nasir, B. J. Lofink, V. H. Santos, H. Patel, X. Peng and L. Sun, *Advanced Composites and Hybrid Materials*, 2018, **1**, 177-184.
46. D. Zhang, B. L. Williams, S. B. Shrestha, Z. Nasir, E. M. Becher, B. J. Lofink, V. H. Santos, H. Patel, X. Peng and L. Sun, *Journal of Colloid and Interface Science*, 2017, **505**, 892-899.
47. L. Sun, W. J. Boo, J. Liu, C.-W. Tien, H.-J. Sue, M. J. Marks and H. Pham, *Polymer Engineering & Science*, 2007, **47**, 1708-1714.
48. W. Huang, S. Zeng, J. Liu and L. Sun, *RSC Advances*, 2015, **5**, 58191-58198.
49. F. Uddin, *Metallurgical and Materials Transactions A*, 2008, **39**, 2804-2814.
50. Y. Xi, R. L. Frost and H. He, *Journal of Colloid and Interface Science*, 2007, **305**, 150-158.
51. X. M. Sun, X. Chen, Z. X. Deng and Y. D. Li, *Materials Chemistry and Physics*, 2003, **78**, 99-104.
52. W. H. Yu, Q. Q. Ren, D. S. Tong, C. H. Zhou and H. Wang, *Applied Clay Science*, 2014, **97-98**, 222-234.
53. L. P. Meier, R. Nueesch and F. T. Madsen, *Journal of Colloid and Interface Science*, 2001, **238**, 24-32.
54. H. J. Ploehn and C. Liu, *Industrial & Engineering Chemistry Research*, 2006, **45**,

7025-7034.
55. R. S. Alvim and C. R. Miranda, *Physical Chemistry Chemical Physics*, 2015, **17**, 4952-4960.
56. L. B. de Paiva, A. R. Morales and F. R. Valenzuela Díaz, *Applied Clay Science*, 2008, **42**, 8-24.
57. M. Shahbabaei and D. Kim, *Physical Chemistry Chemical Physics*, 2017, **19**, 20749-20759.
58. S. Zeng, C. Reyes, J. Liu, P. A. Rodgers, S. H. Wentworth and L. Sun, *Polymer*, 2014, **55**, 6519-6528.
59. H. Sun, J. Zhang, L. Li, J. Xu and D. Sun, *Colloids and Surfaces A: Physicochemical and Engineering Aspects*, 2013, **426**, 26-32.
60. R. C. Rollings, A. T. Kuan and J. A. Golovchenko, *Nature Communications*, 2016, **7**, 11408.
61. J. Gao, W. Guo, D. Feng, H. Wang, D. Zhao and L. Jiang, *Journal of the American Chemical Society*, 2014, **136**, 12265-12272.
62. K. Goh, W. Jiang, H. E. Karahan, S. Zhai, L. Wei, D. Yu, A. G. Fane, R. Wang and Y. Chen, *Advanced Functional Materials*, 2015, **25**, 7348-7359.
63. Y. Feng, M. Weber, C. Maletzko and T.-S. Chung, *Journal of Membrane Science*, 2018, **549**, 550-558.
64. J. A. Lee, M. K. Shin, S. H. Kim, H. U. Cho, G. M. Spinks, G. G. Wallace, M. D. Lima, X. Lepró, M. E. Kozlov, R. H. Baughman and S. J. Kim, *Nature Communications*, 2013, **4**, 1970.
65. H. Huang, Y. Mao, Y. Ying, Y. Liu, L. Sun and X. Peng, *Chemical Communications*, 2013, **49**, 5963-5965.
66. L. Sun, H. Huang and X. Peng, *Chemical Communications*, 2013, **49**, 10718-10720.
67. S. Kandambeth, B. P. Biswal, H. D. Chaudhari, K. C. Rout, S. Kunjattu H., S. Mitra, S. Karak, A. Das, R. Mukherjee, U. K. Kharul and R. Banerjee, *Advanced Materials*, 2017, **29**, 1603945.
68. Y. Han, Z. Xu and C. Gao, *Advanced Functional Materials*, 2013, **23**, 3693-3700.
69. M. Hu and B. Mi, *Environmental Science & Technology*, 2013, **47**, 3715-3723.
70. S. K. Kannam, B. D. Todd, J. S. Hansen and P. J. Daivis, *The Journal of Chemical Physics*, 2011, **135**, 144701.
71. R. R. Nair, H. A. Wu, P. N. Jayaram, I. V. Grigorieva and A. K. Geim, *Science*, 2012, **335**, 442-444.